Structural relaxation in super-cooled water by time-resolved spectroscopy

7. Pohl, M. Limits for an inverse bremsstrahlung origin of the diffuse Galactic soft gamma-ray emission. *Astron. Astrophys.* **339,** 587–590 (1998).
8. Dogiel, V. A., Inoue, H., Schönfelder, V. & Strong, A. W. The origin of diffuse X-ray emission from the Galactic ridge. I. Energy output of particle sources. *Astrophys. J.* **581,** 1061–1070 (2002).
9. Webber, W. R. in *Composition and Origin of Cosmic Rays* (ed. Shapiro, M. M.) 83–100 (Boston, Dordrecht, 1983).
10. Skibo, J. G., Ramaty, R. & Purcell, W. R. Implications of the diffuse Galactic continuum. *Astron. Astrophys. Suppl. Ser.* **120,** 403–406 (1996).
11. Lebrun, F. *et al.* Nature of the Galactic soft gamma-ray emission. *Astrophys. Lett. Commun.* **38,** 457–460 (1999).
12. Winkler, C. *et al.* The INTEGRAL mission. *Astron. Astrophys.* **411,** L1–L6 (2003).
13. Ubertini, P. *et al.* IBIS: the imager on-board INTEGRAL. *Astron. Astrophys.* **411,** L131–L139 (2003).
14. Vedrenne, G. *et al.* The spectrometer aboard INTEGRAL. *Astron. Astrophys.* **411,** L63–L70 (2003).
15. Lebrun, F. *et al.* ISGRI: the INTEGRAL Soft Gamma-Ray Imager. *Astron. Astrophys.* **411,** L141–L148 (2003).
16. Goldwurm, A. *et al.* The INTEGRAL/IBIS scientific data analysis. *Astron. Astrophys.* **411,** L223–L229 (2003).
17. Walter, R. *et al.* INTEGRAL discovery of a bright highly obscured galactic X-ray binary source IGR J16318–4848. *Astron. Astrophys.* **411,** L427–L432 (2003).
18. Strong, A. W. *et al.* Diffuse continuum emission from the inner Galaxy: first results from INTEGRAL/SPI. *Astron. Astrophys.* **411,** L447–L450 (2003).
19. Wang, Q. D., Gotthelf, E. V. & Lang, C. C. A faint discrete source origin for the highly ionized iron emission from the Galactic centre region. *Nature* **415,** 148–150 (2002).
20. Gros, A. *et al.* The INTEGRAL IBIS/ISGRI point spread function and source location accuracy. *Astron. Astrophys.* **411,** L179–L183 (2003).

Acknowledgements This paper is based on observations with INTEGRAL, an ESA project with instruments and science data centre funded by ESA member states (especially the PI countries: Denmark, France, Germany, Italy, Switzerland and Spain), the Czech Republic and Poland, and with the participation of Russia and the USA. We thank CNES for its support during the ISGRI development and in the INTEGRAL data analysis.

Competing interests statement The authors declare that they have no competing financial interests.

Correspondence and requests for materials should be addressed to F.L. (flebrun@cea.fr).

Structural relaxation in supercooled water by time-resolved spectroscopy

Renato Torre[1,2,3], **Paolo Bartolini**[1,2] **& Roberto Righini**[1,2,4]

[1]*European Laboratory for Non-linear Spectroscopy,* [2]*Instituto Nazionale per la Fisica della Materia,* [3]*Dipartimento di Fisica, and* [4]*Dipartimento di Chimica, Università di Firenze, Polo Scientifico, Sesto Fiorentino, Firenze, 50019 Italia*

Water has many kinetic and thermodynamic properties that exhibit an anomalous dependence on temperature[1–5], in particular in the supercooled phase. These anomalies have long been interpreted in terms of underlying structural causes, and their experimental characterization points to the existence of a singularity at a temperature of about 225 K. Further insights into the nature and origin of this singularity might be gained by completely characterizing the structural relaxation in supercooled water[6]. But until now, such a characterization has only been realized in simulations[7–9] that agree with the predictions of simple mode-coupling theory[10]; unambiguous experimental support for this surprising conclusion is, however, not yet available[11–14]. Here we report time-resolved optical Kerr effect measurements[15] that unambiguously demonstrate that the structural relaxation of liquid and weakly supercooled water follows the behaviour predicted by simple mode-coupling theory. Our findings thus support the interpretation[7–9] of the singularity as a purely dynamical transition. That is, the anomalous behaviour of weakly supercooled water can be explained using a fully dynamic model and without needing to invoke a thermodynamic origin. In this regard, water behaves like many other, normal molecular liquids that are fragile glass-formers.

The shear viscosity, self-diffusion coefficient and relaxation times of water above melting and in the supercooled state all exhibit a temperature dependence following a diverging power law[1–5] of the type $(T/T_S - 1)^{-x}$, independent of the measurement method used. Thermodynamic properties such as heat capacity, compressibility and thermal expansion coefficient similarly show a temperature dependence characterized by an anomalous increase upon cooling. Different experimental determinations of the singularity temperature T_S converge on values of about 223–228 K. Although the nature and physical origin of this singularity are still debated[16–18], the observed anomalous phenomena suggest that modifications of structural properties of water occur around this temperature. Characterizing the correlation functions of water and their time evolution, at temperatures below melting and approaching T_S, might therefore yield new insights. But although simulation results suggest that the features of the investigated dynamic correlation functions agree well with the predictions of mode-coupling theory[7–9], unambiguous experimental support for this surprising conclusion is not yet available[11–14].

Several recent time-resolved optical Kerr effect (OKE) experiments on water have revealed[11,19–23] an oscillation on short timescales (for delay time shorter than 1 ps) in the time profile of the measured signal; at longer times, the signal shows a monotonous

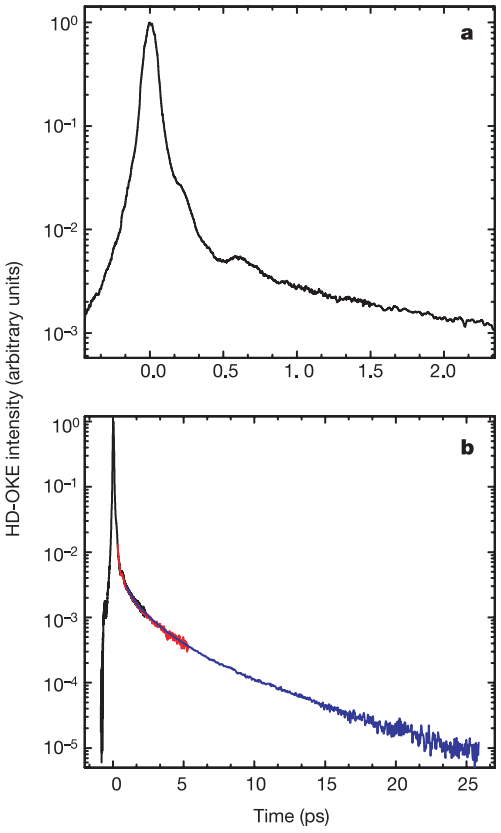

Figure 1 Signal decay measured in the time-resolved HD-OKE experiment on supercooled water at $T = 257$ K. **a**, HD-OKE signal in the short time region. An oscillatory component occurs in the decay trace for time shorter than 1 ps. **b**, HD-OKE signal over the whole time region measured. For longer time the relaxation shows a monotonous decay. The plot illustrates the procedure used for improving the sensitivity. The entire time decay scan was divided into three sections. Short laser pulses (60 fs) were used for the short time scan (black line); for the intermediate time delay intervals (red line) the laser pulse duration was stretched up to 120 fs; for the longer time (blue line) we used stretched laser pulses of 500 fs duration. In this procedure we increased the pulse energy to keep the peak power roughly constant. Care was taken to ensure a large time overlap between subsequent scans, to allow an accurate rescaling of the intensities and a proper reconstruction of the entire decay curve.

decay for which various interpretations have been proposed. The oscillatory part of the signal shows a limited dependence on temperature, while the long time decay slows down as temperature is lowered. So far, attention has mostly focused on the initial oscillatory component of the OKE signal, which provides information about intermolecular hydrogen-bond dynamics and might be directly compared with the low-frequency Raman spectra. But this focus also reflects practical considerations: the intensity of the OKE signal of water is very low, making it very difficult to determine its relaxation profile accurately at times longer than a very few picoseconds.

Here we present the results of an extensive investigation by means of heterodyne detected OKE experiments (HD-OKE) of the relaxation in liquid and supercooled water, using the experimental set-up described in ref. 24. The low noise level and the large dynamic range provide data of sufficiently high quality to extend measurements by almost twenty degrees into the supercooled region. The procedure adopted in our experiments is based on the use of laser pulses of variable duration and energy (see Fig. 1). It allows us to measure the OKE signal relaxation over a large time interval: at the lowest temperature (254 K), we follow the decay of the OKE signal over 40 ps. We can thus provide the first unambiguous measurement of the entire correlation function in liquid water and perform a full mode-coupling theory (MCT) analysis of the slow dynamic regime.

An important aspect to be considered in interpreting OKE and depolarized light-scattering experiments on liquid water is the microscopic origin of the measured signal. The molecular polarizability of water is almost isotropic and the optically induced polarization is therefore dominated by intermolecular (collision-induced) contributions. This holds not only for the high-frequency ($>10\,cm^{-1}$) part of the light-scattering spectrum (corresponding to the short time OKE signal), but also for the very-low-frequency part[25] that corresponds to the long time relaxation tail of our time-domain data. In other words, the OKE and depolarized-light-scattering techniques are mostly sensitive to the intermolecular dynamics of water. In the short delay time limit, this corresponds to the intracage vibrational dynamics; the long time decay, in contrast, is prevalently associated with rearrangement of local (cage) structures, which represents the first step of the overall structural relaxation. More precisely, the measured signal in a OKE experiment is defined by the material response function[15], that is, by the time-derivative of the dielectric-constant correlation function[26,27] which, in water, is dominated by the intermolecular contribution.

Figure 2a collects several HD-OKE data measured at different temperatures (314–254 K). The log–log plots clearly show the marked slowing down with decreasing temperature of the overall relaxation, and the slight temperature dependence of the fast

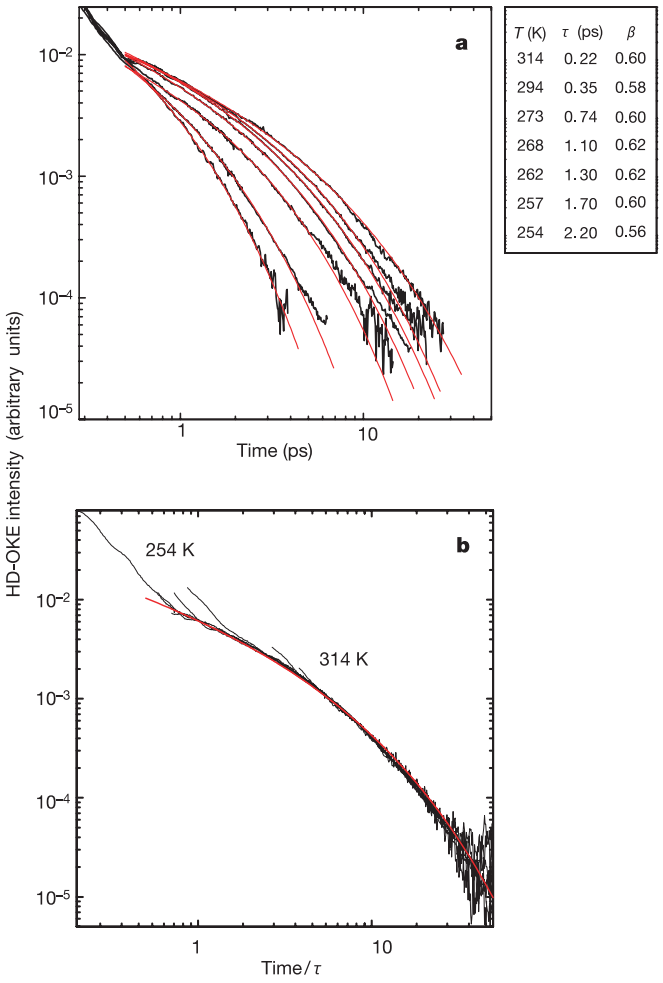

T (K)	τ (ps)	β
314	0.22	0.60
294	0.35	0.58
273	0.74	0.60
268	1.10	0.62
262	1.30	0.62
257	1.70	0.60
254	2.20	0.56

Figure 2 Temperature dependence of the HD-OKE signals on water and fits based on the stretched exponential function. **a**, A log–log plot of the HD-OKE signals as a function of the temperature. The red curves are best fits performed with the time-derivative of the stretched exponential function; the values of the τ and β parameters are listed. **b**, Master plot obtained by rescaling the time and intensity axes of the HD-OKE signals showed in **a**; the reported red line is the master curve corresponding to the time-derivative of the stretched exponential with $\tau = 1$ and $\beta = 0.6$.

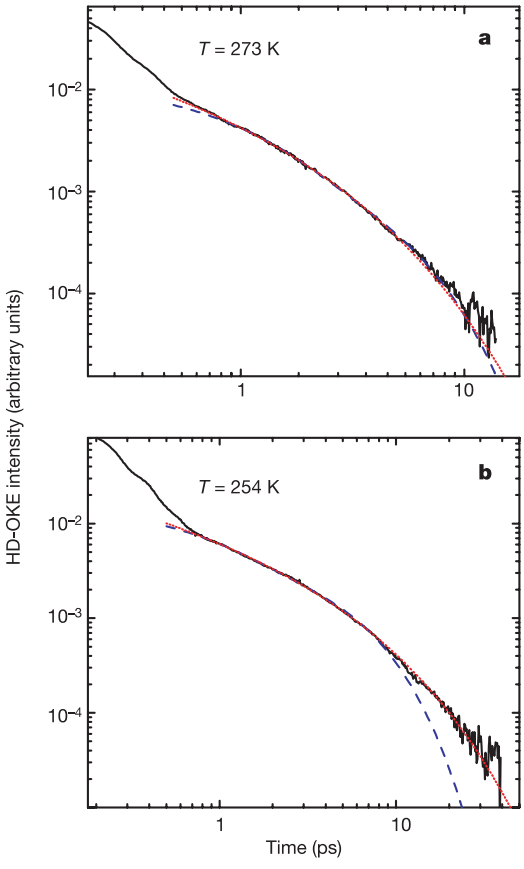

Figure 3 HD-OKE signals on liquid and supercooled water with a detailed analysis of the relaxation time profile. **a**, HD-OKE signal at $T = 273$ K. The difference between fits performed with the time-derivative of the double exponential (blue dashed line) and time-derivative of the stretched exponential (red dotted line) is hardly observable owing to the noise and time limitations. **b**, HD-OKE signal at $T = 254$ K. The time-derivative of the double exponential curve (blue dashed line) is clearly unable to reproduce the data for time delays longer than 8 ps—instead the time-derivative of the stretched exponential function is able to fully fit the experimental decay in the complete time region investigated.

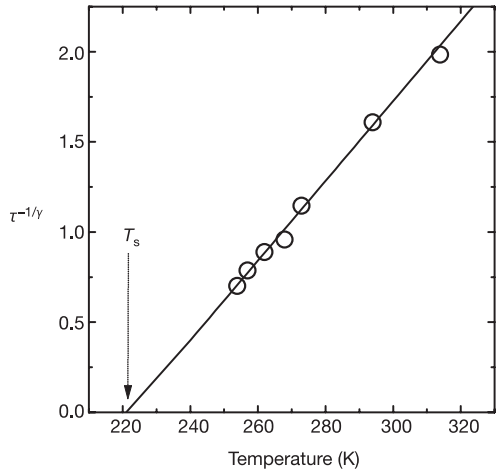

Figure 4 Temperature dependence of the water relaxation times, obtained by the fit of HD-OKE signal decays with the time-derivative of the stretched exponential function. The relaxation times in Fig. 2 follow the power law $\tau(T) = a(T - T_S)^{-\gamma}$ with $T_S = 221 \pm 5$ K and $\gamma = 2.2 \pm 0.3$. Here we reported the data (open circles) and the fit (continuous line) in a linearized plot, $\tau^{-1/\gamma}$ versus T. This plot shows clearly the linear dependence of the renormalized times and the T_S value supported by the fit. The T_S and γ values are in agreement with the MCT, so our data support the equivalence of the singularity temperature T_S with the dynamical critical temperature predicted by the MCT.

component (for $\tau < 1$ ps). Figure 2b shows the master plot obtained from the data of Fig. 2a by rescaling the time and amplitude axes of each curve. The perfect coincidence of the different curves demonstrates that the slow relaxation of water follows a unique decay law in the entire temperature range considered. We found, for all the temperatures, that the time-derivative of the stretched exponential function, $f(t) = -\mathrm{d}/\mathrm{d}t \ \exp(-(t/\tau)^{\beta})$, allows a very satisfactory fitting of the HD-OKE data: the values of the parameters τ and β obtained at the different temperatures are collected in the box of Fig. 2a.

The comparison of the two fittings in Fig. 3 clearly demonstrates that at 273 K, the difference between a double exponential and a stretched exponential function is hardly detectable owing to the limited time interval explored. At 254 K, on the other hand, the wider time window accessible to the experiment shows that the double exponential function is unable to account for the OKE signal decay in the last 20 ps.

A second important conclusion from the data of Fig. 2a is that the stretching parameter β has a constant value of 0.6 throughout the entire temperature range considered.

As shown in Fig. 4, the temperature dependence of the measured relaxation time τ is well reproduced by a power law of the type $\tau(T) = a(T - T_S)^{-\gamma}$. The best fit is obtained using values of $T_S = 221 \pm 5$ K and $\gamma = 2.2 \pm 0.3$ for the power-law parameters. The T_S we obtain thus coincides with the singularity temperature obtained from measurements of other dynamic and transport properties.

The two important new results obtained from our OKE experiment are the stretched exponential nature of the relaxation and the invariance of the stretching parameter with the temperature. The large stretching effect ($\beta = 0.6$) indicates that water dynamics is characterized by a distribution of different timescales, suggesting the presence of a variety of relaxing structures[6] whose distribution does not, according to our results, change notably with temperature.

Our data also allow for a comprehensive comparison with the predictions of simple MCT[10] concerning the slow dynamics in liquid water. MCT, which is a dynamic model providing a description of the temporal evolution of the correlation functions related to density, predicts that the long time decay (α relaxation) follows a stretched exponential law with a temperature-independent stretching parameter. Furthermore, the α relaxation time increases on cooling according to a power law, from which a critical temperature T_S can be derived. These predictions fully agree with our experimental observations. In the simple MCT, T_S represents the temperature of dynamical structural arrest, although recently extended versions propose a new definition of T_S, involving a crossover or avoided-singularity temperature corresponding to a sudden variation of the dynamic nature of the supercooled liquid.

A purely dynamic water model clearly cannot account for the rich and anomalous thermodynamic behaviour of water, which calls for other model types such as the much debated[16–18] second critical point hypothesis[28] (SCP). But the predictions of thermodynamic models usually do not cover dynamic properties, such as the temporal evolution of the correlation functions we have measured. Although some recent computer simulations[29] attempt to bridge this gap, we are at present unable to compare our experimental results directly against the predictions of thermodynamic models such as the SCP hypothesis.

On the other hand, our data fully support the MCT scenario, both in terms of the form of the correlation function and in terms of its scaling with temperature. This agreement provides unambiguous evidence that the anomalous behaviour of weakly supercooled water at atmospheric pressure can successfully be described by a fully dynamic model, with no need for a thermodynamic origin for the observed anomalous behaviour. In this picture the singularity temperature T_S, inferred from a range of different dynamic and transport properties of water, is the signature of an avoided dynamical arrest. Despite its strongly hydrogen-bonded nature, weakly supercooled water behaves in this context like a fragile glass-former, as seen for many other molecular liquids. □

Received 31 October 2003; accepted 4 February 2004; doi:10.1038/nature02409.

1. Angell, C. A. in *Water: A Comprehensive Treatise* (ed. Franks, F.) Vol. 7 1–81 (Plenum, New York, 1982).
2. Angell, C. A. Supercooled water. *Annu. Rev. Phys. Chem.* **34,** 593–630 (1983).
3. Mishima, O. & Stanley, H. E. The relationship between liquid, supercooled and glassy water. *Nature* **396,** 329–335 (1995).
4. Debenedetti, P. G. *Metastable Liquids* Ch. 4 305–335 (Princeton Univ. Press, Princeton, 1996).
5. Speedy, R. J. & Angell, C. A. Isothermal compressibility of supercooled water and evidence for thermodynamic singularity at −45°C. *J. Chem. Phys.* **65,** 851–858 (1976).
6. Debenedetti, P. G. & Stillinger, F. H. Supercooled liquids and the glass transition. *Nature* **401,** 259–267 (2001).
7. Sciortino, F., Gallo, P., Tartaglia, P. & Chen, S.-H. Supercooled water and the kinetic glass transition. *Phys. Rev. E* **54,** 6331–6343 (1996).
8. Fabbian, L. *et al.* Molecular mode coupling theory for supercooled liquids: Application to water. *Phys. Rev. E* **60,** 5768–5777 (1999).
9. Sciortino, F. Slow dynamics in supercooled water. *Chem. Phys.* **258,** 307–314 (2000).
10. Götze, W. & Sjögren, L. Relaxation processes in supercooled liquids. *Rep. Prog. Phys.* **55,** 241–336 (1992).
11. Winkler, K., Lindner, J., Bürsing, H. & Vöringer, P. Ultrafast Raman-induced Kerr-effect of water: Single molecule versus collective motions. *J. Chem. Phys.* **113,** 4674–4682 (2000).
12. Rønne, C., Åstrand, P.-O. & Keiding, S. R. THz spectroscopy of liquid H_2O and D_2O. *Phys. Rev. Lett.* **82,** 2888–2891 (1999).
13. Sokolov, A. P., Hurst, J. & Quitmann, D. Dynamics of supercooled water: Mode-coupling theory approach. *Phys. Rev. B* **51,** 12865–12868 (1995).
14. Bellisent-Funel, M. C., Longeville, S., Zanotti, J. M. & Chen, S.-H. Experimental observation of the α relaxation in supercooled water. *Phys. Rev. Lett.* **85,** 3644–3647 (2000).
15. Righini, R. Ultrafast optical Kerr effects in liquids and solids. *Science* **262,** 1386–1390 (1993).
16. Debenedetti, P. G. & Stanley, H. E. Supercooled and the glassy water. *Phys. Today* **56,** 40–46 (2003).
17. Sciortino, F., La Nave, E. & Tartaglia, P. Physics of the liquid-liquid critical point. *Phys. Rev. Lett.* **91,** 155701 (2003).
18. Franzese, G., Marqués, M. I. & Stanley, H. E. Intramolecular coupling as a mechanism for a liquid-liquid phase transition. *Phys. Rev. E* **67,** 011103 (2003).
19. Castner, E. W., Chang, Y. J., Chu, Y. C. & Walrafen, G. E. The intermolecular dynamics of liquid water. *J. Chem. Phys.* **102,** 653–659 (1995).
20. Palese, S., Schilling, L., Miller, R. J. D., Staver, P. R. & Lotshaw, W. T. Femtosecond optical Kerr-effect studies of water. *J. Phys. Chem.* **98,** 6308–6316 (1994).
21. Palese, S., Mukamel, S., Miller, R. J. D. & Lotshaw, W. T. Interrogation of vibrational structure and line broadening of liquid water by Raman-induced Kerr-effect measurements within the multimode Brownian oscillator model. *J. Phys. Chem.* **100,** 10380–10388 (1996).
22. Foggi, P., Bellini, M., Kien, D. P., Vercuque, I. & Righini, R. Relaxation dynamics of water and HCl aqueous solutions measured by time-resolved optical Kerr effect. *J. Phys. Chem.* **101,** 7029–7035 (1997).

23. Winkler, K., Lindner, J. & Vöringer, P. Low frequency depolarized Raman-spectral density of liquid water from femtosecond optical Kerr-effect measurements: Lineshape analysis of restricted translational modes. *Phys. Chem. Chem. Phys.* **4,** 2144–2155 (2002).
24. Bartolini, P., Ricci, M., Torre, R. & Righini, R. Diffusive and oscillatory dynamics of iodobenzene measured by femtosecond optical Kerr effect. *J. Chem. Phys.* **110,** 8653–8662 (1999).
25. Ricci, M. A., Ruocco, G. & Sampoli, M. Raman spectra of water in the translational and librational regions. III — Temperature evolution by computer simulation with the TIP4P potential. *Mol. Phys.* **67,** 19–31 (1989).
26. Torre, R., Bartolini, P. & Pick, R. M. Time-resolved optical Kerr effect in a fragile glass-forming liquid, salol. *Phys. Rev. E* **57,** 1912–1920 (1998).
27. Torre, R., Bartolini, P., Ricci, M. & Pick, R. M. Time-resolved optical Kerr effect in a fragile glass-forming liquid: Test of different mode coupling theory aspects. *Europhys. Lett.* **52,** 324–329 (2000).
28. Poole, P. H., Sciortino, F., Essmann, U. & Stanley, H. E. Phase behaviour of metastable water. *Nature* **360,** 324–328 (1992).
29. Sastry, S. & Angell, C. A. Liquid-liquid phase transition in supercooled silicon. *Nature Mater.* **2,** 739–743 (2003).

Acknowledgements This work was supported by INFM, by the FIRB and COFIN programmes of Italian MIUR, and by an EC grant. We thank F. Sciortino, C. A. Angell and G. Ruocco for discussions.

Competing interests statement The authors declare that they have no competing financial interests.

Correspondence and requests for materials should be addressed to R.T. (torre@lens.unifi.it).

High-mobility ultrathin semiconducting films prepared by spin coating

David B. Mitzi, Laura L. Kosbar, Conal E. Murray, Matthew Copel & Ali Afzali

IBM T. J. Watson Research Center, PO Box 218, Yorktown Heights, New York 10598, USA

The ability to deposit and tailor reliable semiconducting films (with a particular recent emphasis on ultrathin systems) is indispensable for contemporary solid-state electronics[1–3]. The search for thin-film semiconductors that provide simultaneously high carrier mobility and convenient solution-based deposition is also an important research direction, with the resulting expectations of new technologies (such as flexible or wearable computers, large-area high-resolution displays and electronic paper) and lower-cost device fabrication[4–11]. Here we demonstrate a technique for spin coating ultrathin (~50 Å), crystalline and continuous metal chalcogenide films, based on the low-temperature decomposition of highly soluble hydrazinium precursors. We fabricate thin-film field-effect transistors (TFTs) based on semiconducting $SnS_{2-x}Se_x$ films, which exhibit n-type transport, large current densities (>10^5 A cm^{-2}) and mobilities greater than 10 cm^2 V^{-1} s^{-1}—an order of magnitude higher than previously reported values for spin-coated semiconductors. The spin-coating technique is expected to be applicable to a range of metal chalcogenides, particularly those based on main group metals, as well as for the fabrication of a variety of thin-film-based devices (for example, solar cells[12], thermoelectrics[13] and memory devices[14]).

Recent research on solution-processed semiconducting films has primarily focused on organic systems[4–9], with mobilities as high as 0.89 cm^2 V^{-1} s^{-1} reported for p-type TFT channels composed of solution-processed pentacene[6]. Analogous n-type materials have proved more challenging, and have generally yielded much lower mobilities[8,9]. Although promising with regard to processing, cost and weight considerations, the weak van der Waals interaction between organic moieties imposes an upper bound on mobility[9], thereby limiting organic semiconductors to lower-end applications. Spin-coated organic–inorganic hybrid films have also recently been used as the semiconducting element in TFTs[10,11], yielding saturation regime mobilities as high as 1 cm^2 V^{-1} s^{-1} (ref. 11). Although promising, current tin(II)-iodide-based hybrids are air-sensitive, requiring all processing and characterization to be performed under rigorously inert atmospheric conditions. Additionally, although the pentacene and tin(II)-iodide-based systems are p-type, n-type analogues are also desirable to enable applications involving complementary logic.

Metal chalcogenide films provide an opportunity for higher mobility than the organic and hybrid semiconductors, as a result

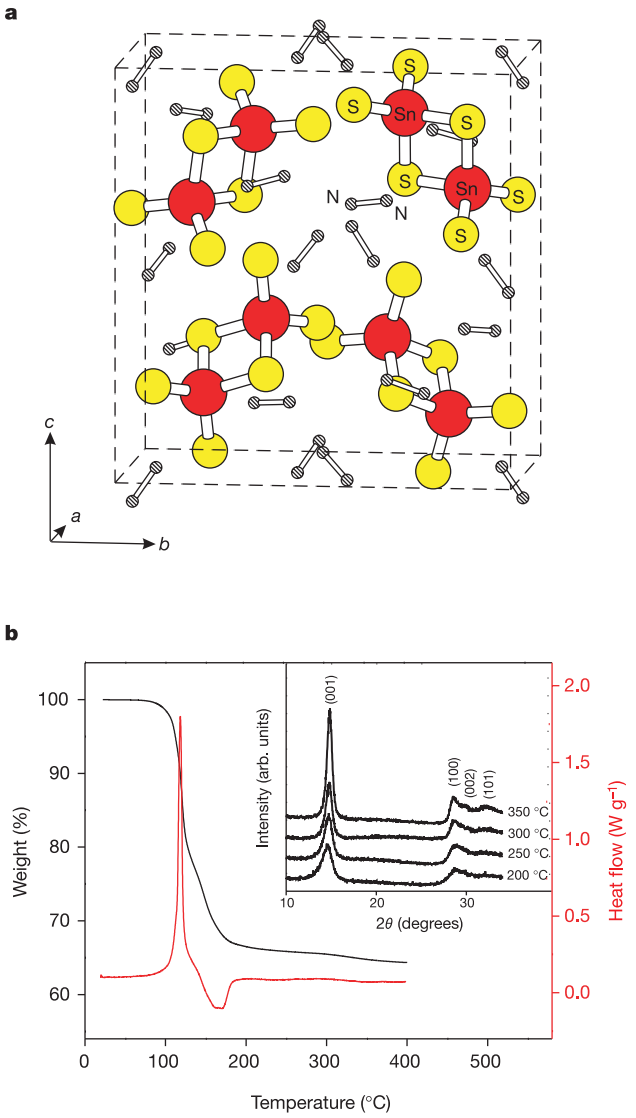

Figure 1 Crystal structure and thermal properties of the hydrazinium precursor. **a**, Crystal structure of $(N_2H_5)_4Sn_2S_6$, determined using single-crystal X-ray diffraction. Hydrogen atoms are not shown for clarity. Unit cell (outlined by dashed lines): orthorhombic ($P2_12_12_1$), a = 8.5220(5) Å, b = 13.6991(8) Å, c = 14.4102(9) Å, V = 1,682.3(2) Å^3 and Z = 4. Further details of the structure determination for both $(N_2H_5)_4Sn_2S_6$ and the analogous selenide precursor will be published elsewhere. **b**, Thermogravimetric analysis (TGA) and differential scanning calorimetry (DSC) scans for the $(N_2H_5)_4Sn_2S_6$ precursor (2 °C min^{-1} ramp rate). Exothermal peaks are down along the heat flow axis. Inset, the powder X-ray diffraction pattern for the precursor after a TGA run terminated at various temperatures (200–350 °C) (listed along the right side of the plot), demonstrating good agreement with the expected diffraction pattern for SnS_2 (berndtite, PDF 23-0677; the reflection indices are shown in parentheses).